Combining Magnetic Induction Tomography and Electromagnetic Velocity Tomography for Water Continuous Multiphase Flows

Lu Ma, Dominic McCann, and Andrew Hunt

***Abstract*— For oil fields producing high fractions of water, it is critical to be able to accurately meter the water volumetric flowrate for production allocation and field life optimization. This paper reports the measurement principles and experimental results of a multiphase flow meter prototype, capable of non-intrusively measuring the water volumetric flowrate in a multiphase flow. This research prototype is based on a novel concept of combining two tomographic systems—magnetic induction tomography and electromagnetic velocity tomography—for measuring the cross-sectional volumetric fraction and the local axial velocity of the water phase, respectively. The fundamental principles and imaging capability of each technique are shown. First impressions of the prototype performance are demonstrated using experimental data from an in-house flow loop. The challenges and potential improvements are also addressed.**

***Index Terms*— Multiphase flow, magnetic induction tomography, electromagnetic velocity tomography.**

I. Introduction

THE current generation of multiphase flow meters typically use a combination of gamma-ray densitometers, venturi meters and other sampling techniques to measure the flowrate of each phase in a multiphase flow. However, there is a pressing need for the development of a fully electrical-based and non-intrusive flow measurement technique in various types of multiphase flow. This is particularly true for obtaining accurate measurements of the volumetric flowrate of the water phase in water continuous multiphase flows, a type of flow which is frequently encountered in the oil industry. In order to measure the volumetric flowrate of the water phase, the product of the water volumetric fraction and local water velocity must be integrated in the flow cross-section.

The combined use of two such techniques is described here: magnetic induction tomography (MIT), and electromagnetic velocity tomography (EVT). This combination gives an instantaneous measurement of the water volumetric fraction and velocity distribution, allowing accurate metering of water flow in complex multiphase conditions.

Many electrical methods have been developed for flow measurement due to their low cost, fast response and easy installation character. The electrical methods are usually based on either impedance, capacitance or electromagnetic measurements. Of these, MIT, a type of electromagnetic tomographic technique, has gained increasing research interest for the visualisation of a conducting phase in a multiphase flow. Due to its contactless and non-invasive nature, MIT has advantages in determining the volumetric fraction of the water phase compared to electrical resistance tomography, which often requires direct electrode contact with the flow [1], [2]. Contactless capacitance methods have also been commonly used for two-phase flow measurement [3], however is not applicable when the conducting phase is continuous. Various conductance probes have the capability of measuring the water volumetric fraction in a two phase flow [4]–[6], but due to the lack of local velocity information, the water flowrate cannot be directly obtained. Previous studies of MIT, analysing mixtures of water-oil and water-air, used either simulation models or static phantom tests to replicate various flow conditions [7]–[10]. These studies showed that the electromagnetic field induced due to saline conductivity can be sensed by inductive coils, and that the distribution of saline water can be measured and reconstructed via this tomographic approach. Studies on the use of MIT for metallurgical applications, such as the characterisation of two-phase metal flows, have been reported in [11] and [12]; these flows have different characteristics (state change due to temperature change during solidification process) and electrical properties (a much higher conductivity value than that of water in a multiphase flow in the oil and gas industry, with the latter being the subject of this study). In our study, the primary focus is the measurement of water volumetric flowrate in water and oil flows. There are only two phases involved: water is the continuous and conducting phase, and oil is the discontinuous and non-conducting phase. Hence MIT can be used to distinguish between the two and the water volumetric fraction necessary for calculating flowrate can be derived.

Electromagnetic velocity measurement techniques have evolved significantly, from the traditional electromagnetic flow meter (which uses a pair of electrodes to measure a cross-sectional velocity in axisymmetric flows [13], to multi-electrode measurements of the mean velocity of highly

Manuscript received July 29, 2017; revised September 6, 2017; accepted September 23, 2017. Date of publication October 9, 2017; date of current version November 22, 2017. The associate editor coordinating the review of this paper and approving it for publication was Dr. Chao Tan. *(Corresponding author: Lu Ma.)*

L. Ma is with the Engineering Tomography Laboratory, Department of Electronic and Electrical Engineering, University of Bath, Bath BA2 7AY, U.K. (e-mail: l.ma@bath.ac.uk).

D. McCann is with the iPhase Ltd., Oxford OX1 5DL, U.K. (e-mail: dominicmccann@iphaseflow.com).

A. Hunt is with the Flow Measurement and Fluid Mechanics Research Center, Faculty of Engineering and Computing, Coventry University, Coventry CV1 5FB, U.K. (e-mail: andrew.hunt@coventry.ac.uk).

Digital Object Identifier 10.1109/JSEN.2017.2758601

asymmetric single phase flows [14] and of the local velocity distribution in either axisymmetric or asymmetric multiphase flows [15]–[17]. Among the multi-electrode electromagnetic flow meters, EVT is the most recently developed, capable of measuring and reconstructing an image of the water velocity distribution across the whole pipe area, especially those distributions with non-uniform axial velocities [18]. These capabilities distinguish the implementation of EVT from other electromagnetic meters. A combination of EVT and an impedance cross correlation (ICC) method has been studied to determine the water and solid volumetric flowrates in stratified, inclined solids-in-water flows [19]. In addition, the solids volumetric fraction obtained using ICC was compared with a differential pressure (DP) method, showing a good agreement between the two, ultimately resulting in a flowrate calculation with $\pm 10\%$ relative error if using a combination of EVT and ICC. This work is encouraging in that it provides an evidential basis for combining two techniques - one for the measurement of volumetric velocity, and one for the measurement of volumetric fraction - to calculate the flowrate of one phase in a multiphase flow.

This paper introduces the combination of MIT and EVT to calculate the water volumetric flowrate in water continuous multiphase flows. To the best of our knowledge, this is the first study of this type, presenting the following advances on previous published work: (i) the flow measurement and evaluation are performed in real time on multiphase flows, (ii) the reconstructed images of the distribution of the water and the velocity of that phase are presented for a given multiphase flow condition over the same sampling period, (iii) the integration of the MIT and EVT measurements can be used to calculate the water volumetric flowrate, and to estimate the slip velocity and the distribution of the flow profile in a water continuous multiphase flow.

II. Methods

A. Electromagnetic Considerations for Flow Measurement

Although EVT and MIT both measure induced voltages using electrodes or inductive coils, it is important to note that these induced voltage measurements have different natures. The induced voltages measured by EVT and MIT are referred to the motional and inductive electromotive forces, respectively, due to the velocity and electrical properties of a conducting flow. The governing equation of a combination of EVT and MIT can be written as:

$$\nabla \times H = \sigma (\upsilon \times B) + \sigma E' + J_s \tag{1}$$

where H is the magnetic field intensity, σ is the conductivity of the conducting phase, υ is the velocity of the conducting phase, B is the applied magnetic field flux density from a EVT system. This B field neither depends on nor contains any flow information. E' is the total electric field caused by both the motional and inductive electromotive forces. J_s is the excitation current source provided to the inductive coils. It can be seen that the conductivity and velocity distribution of the conducting flow cannot be solved from one equation. In the case of MIT, the sensitivity formulation usually focuses on the relationship of the induced voltages and the conductivity distribution, with the imaging subject considered to be static (i.e., $\upsilon = 0$) compared to the changing rate of the J_s induced AC field [20]. The motional electromotive force is negligible, therefore equation 1 is simplified as equation 2. In the case of EVT, $J_s = 0$. The term $\sigma E'$ is the ohmic current, containing the current generated by the eddy currents induced-magnetic field in the electrodes. The applied B is much larger than the flow-induced magnetic field, only the motional electromotive force component in E' is considered, therefore equation 1 is simplified as equation 5.

B. MIT Principles

MIT utilises an array of inductive coils, distributed equally around a pipe periphery, to visualise the electromagnetic property distribution of a conducting phase inside a pipe. The imaging principle is based on the laws of induction and eddy currents which are induced in an AC magnetic field. The governing equation can be written as equation 2, where σ_e is the conductivity distribution.

$$\nabla \times H = J_s + \sigma_e E \tag{2}$$

The governing equation 2 can also be formulated in terms of E field. For each transmitter and receiver coil combination, the sensitivity coefficient is given by equation 3, where E_i is the induced electric field in a given pixel when one transmitter coil i is excited by a source current. Similarly, E_j is the induced electric field when coil j is excited and the dot product of the two electric field vectors E_i and E_j is integrated over the area of the pixel. The set of sensitivity coefficients for each coil-pair is known as the sensitivity map for that pair. Hence the sensitivity matrix can be considered to be formed from M sensitivity maps, one for each measurement pair. The E field is calculated analytically using the conjugate harmonic method for a circular geometry with a high degree of symmetry [21].

$$S = \int_A E_i \cdot E_j dA \tag{3}$$

The inverse problem can be written as equation 4, where b is a column vector comprising a total number of M changes of induced voltages, σ_e is also a column vector representing unknown conductivity distribution in a total number of p^2 pixels.

$$b = S\sigma_e \tag{4}$$

As the number of measurements is far lower than the number of pixels, the sensitivity matrix is non-square. The inverse of S does not exist. In this study, when solving σ_e, a linear back projection algorithm is selected due to its fast computation and suitability for real time imaging, in which the transpose of S is used as the pseudo-inverse of S.

C. EVT Principles

The EVT principles also originate from electromagnetic induction. Two Helmholtz coils are placed directly facing each other. By driving these coils, a magnetic field can be generated across the pipe within the flow. When there is

a conducting phase flowing through this field, an electric field can be induced and measured by an array of electrodes in partial contact with the flow. The measured electric potential distributions are dependent on the intensity of the induced electric field, and hence are functions of the velocity of the flow. The governing equation of EVT can be shown as equation 5 [22]:

$$\nabla \times H = \sigma_w E + \sigma_w (v_w \times B) \tag{5}$$

where H is the magnetic field intensity, σ_w and v_w are the conductivity and velocity of the water phase, respectively, and B and E are the applied magnetic flux density and the induced electric field due to the flow. By substituting E field using an scalar electric potential and taking the divergence, the voltage potential U can be solved using equation 6 with appropriate boundary conditions [23].

$$\nabla^2 U = -\nabla \cdot (v_w \times B) \tag{6}$$

Applying a Discrete Fourier Transform (DFT) to the voltage potentials U (a column vector consisting N number of value U_m, with U_m represents the voltage potential measured at the $N-1$ electrode, where $m = 0:1:N-1$, and N is the total number of electrodes), one can obtain a series of complex number $X(n)$, similarly $n = 0:1:N-1$.

$$X(n) = \frac{1}{N} \sum_{n=0}^{N-1} U_m exp(-j(2\pi nm/N)) \tag{7}$$

The overall velocity profile is calculated as a superposition of up to the fourth order of polynomial components of the voltage potentials, as unrealistic spatial variations may be observed for velocity profiles containing components higher than fourth order display [24]:

$$v(x; y) = \sum_{n=0}^{n=4} v_n(x; y) \tag{8}$$

where each order component is defined below (equation 9 to 13), with x, y and R refer to the x-axis, y-axis and the internal radius of the pipe section. The coefficients of the polynomial velocity components are obtained from complex numbers from equation 7. This is an analytical velocity reconstruction method, equivalent to that of the RT#1 reconstruction technique reported in [25].

$$v_0(x; y) = 1 \tag{9}$$

$$v_1(x; y) = 1(\frac{x}{R} cos90^\circ + \frac{y}{R} sin90^\circ) \tag{10}$$

$$v_2(x; y) = 1(\frac{x}{R} cos45^\circ + \frac{y}{R} sin45^\circ)^2 - 0.25 \tag{11}$$

$$v_3(x; y) = 1(\frac{x}{R} cos20^\circ + \frac{y}{R} sin20^\circ)^3 - 0.5 \times (\frac{x}{R} cos20^\circ + \frac{y}{R} sin20^\circ) \tag{12}$$

$$v_4(x; y) = 1(\frac{x}{R} cos0^\circ + \frac{y}{R} sin0^\circ)^4 - 0.75 \times (\frac{x}{R} cos0^\circ + \frac{y}{R} sin0^\circ)^2 + 0.0625 \tag{13}$$

D. Flow Equations

The superficial velocity of one phase in a multiphase flow is the velocity one phase would have if it travelled alone and completely filled the pipe. Therefore, the superficial velocity can be calculated using the volumetric flowrate of that phase divided by the cross-sectional area of the pipe:

$$v_{ws} = Q_w / A_{area} \tag{14}$$

$$v_{os} = Q_o / A_{area} \tag{15}$$

$$v_{ts} = (Q_w + Q_o) / A_{area} \tag{16}$$

where v_{ws}, v_{os} and v_{ts} are the superficial velocities of water, oil and total liquid phases, Q_w and Q_o are the volumetric flowrates of water and oil phases, and A_{area} is the cross-sectional area of the pipe. The water in liquid ratio (WLR) is the ratio of water volume to the total volume of the liquids, also called water cut.

$$WLR = Q_w / (Q_w + Q_o) \tag{17}$$

The in-situ velocity of one phase in a multiphase flow can be calculated by using the superficial velocity divided by the volumetric fraction of that phase.

$$v_w = v_{ws} / \lambda_w \tag{18}$$

$$v_o = v_{os} / \lambda_o \tag{19}$$

In which v_w, v_o are the in-situ velocities of water and oil phases, λ_w, λ_o are the volumetric fraction of water and oil phases. In water and oil flows, the slip velocity is the velocity difference between the water and oil phases.

$$v_s = v_o - v_w \tag{20}$$

The drift flux model of a water-oil flow is shown as [26]:

$$v_o = C_o \cdot v_{ts} + v_s \tag{21}$$

where C_0 is the flow distribution parameter. The power law profile is widely used for the description of the velocity distribution. This model has been shown to have wide application to multiphase flow, but previous work has empirical values for C_0 and v_s. Here we calculate these values from the measured distribution of water velocity:

$$v_{w,ij} / v_{w,max} = (1 - \frac{2r_{ij}}{D})^n \tag{22}$$

where $v_{w,ij}$ is the water velocity at a local pixel, $v_{w,max}$ is the maximum water velocity across the pipe, r_{ij} is the distance from a given pixel to the center of the pipe, D is the diameter of the pipe, and the value of the exponent n describes the flow profile, for instance, a laminar or near-laminar flow would have a value of $n = 1/2$, and for a flow with a parabolic profile, $n = 1/7$. In this study, a range of n values are used to examine the profiles of various multiphase flow.

E. Flow Parameter Measurement

The extended Maxwell-Wagner-Sillars model covers a dielectric particle permittivity in a mixture of media and derives the particle shape functions. Derived from [27]–[29] and first published in [30], this model has proved powerful in

the derivation of the volumetric fraction of the discontinuous phase λ in a multiphase flow using electrical capacitance tomography. More recently, it has been adapted to derive the water volumetric fraction, also known as water holdup, in a multiphase flow using an integrated sensing system [31] in a water-based model presented in a water continuous multiphase flow [32]. The principal characteristic of this model is that the induced voltages are functions of the conductivity of the mixture. This model can be expressed in equation 23.

$$\sigma_e = \sigma_1[1 + N \cdot \lambda \cdot (\sigma_2 - \sigma_1) / (\sigma_2 + (N-1) \cdot \sigma_1 - \lambda \cdot (\sigma_2 - \sigma_1))] \quad (23)$$

where σ_e, σ_1 and σ_2 are the conductivities of the mixture, continuous and discontinuous phases respectively. The parameter N is used to describe the shape of the distribution of the discontinuous phase, also known as the particle fitting parameter. In the case of water continuous water and oil flows, $\sigma_1 = \sigma_w$, and the conductivity of the mixture can be obtained from equation 3 and 4, λ is the volumetric fraction of the discontinuous phase, in the case of water continuous water oil flows, it is the volumetric fraction of the oil phase, i.e., $\lambda = \lambda_o$. The conductivity of the the oil phase is considered to be negligible, and the shape of the oil bubble is assumed to be spherical, i.e., $N = 3$, resulting in equation 24. This is consistent with the derivation of the water volumetric fraction if using an impedance measurement [33].

$$\lambda_o = (2\sigma_w - 2\sigma_e)/(2\sigma_w + \sigma_e) \quad (24)$$

The water volumetric fraction (also known as water holdup) can be written as:

$$\lambda_w = 1 - \lambda_o \quad (25)$$

Hence the volumetric water flowrate in a multiphase flow can be calculated using equation 26:

$$Q_w = \int_A \lambda_{w,ij}\, v_{w,ij}\, dA \quad (26)$$

where A denotes to the cross section area. $\lambda_{w,ij}$ and $v_{w,ij}$ represent the water volumetric fraction and water local velocity at a local region i, j, in which, $v_{w,ij}$ is measured directly from equation 8. The total number of pixels in the whole pipe cross-section is $p \times p$. In theory, MIT is capable of measuring a mixture of multiphase flow as long as there is a conducting phase is present; however, the EVT operates under a water continuous multiphase flow. Thus in this article, we focus on the derivation of the water volumetric flowrate in a water continuous multiphase flow.

F. Tomographic Measurement Process

The implementation of MIT principles for this study can be summarised as follows. Firstly, establishing the forward model with an estimated conductivity distribution and known sensor geometry. The estimation of the initial conductivity value is important. In many cases, one could start from a conductivity of zero, i.e., an empty pipe, and then reconstruct the absolute conductivity value in a non-linear iterative fashion [34]. In this study, the linear projection method is used to avoid variance in image quality resulting from the selection of different relaxation or regularisation parameters, which are required input to other inverse algorithms [35], [36]. Secondly, formulating the sensitivity matrix, which contains information about how the measured trans-impedance between a defined transmitter and receiver coil pair when a change is made to the conductivity distribution of a given pixel inside the circular vessel (from equation 3). Thirdly, reconstructing the true conductivity distribution using actual measured induced voltages from the instrument for a given flow condition (equation 4). To do so, a measurement calibration is implemented, i.e., the induced voltages measured against an empty pipe is used as reference point. By flowing the entire pipe with different conductive fluids with known conductivity values, the relationship between the conductivity, volume and induced voltages can then be derived. For flow conditions considered in this study, as the conductivity of the saline water is a known parameter, the volume is the parameter that needs to be solved. It has been shown that for conductivities lower than 10 S/m, the induced voltage (phase component) is known to have a linear relationship with the conductivity in a static phantom test. Due to the motional force between different constituencies in a multiphase flow, the extended Maxwell-Wagner-Sillars model offers the additional flexibility of taking into account the effect of the particle shape for this calibration process (equation 23). Finally, deriving the volumetric fraction of the conducting phase from the reconstructed conductivity distribution (equation 25).

The implementation of EVT principles can be summerised in three steps. Firstly, by applying an external magnetic field to a flow surrounded by a given electrode array, the induced voltage potential can be calculated (equation 6). Secondly, by applying a DFT method to the measured voltage potentials, its complex numbers provide the information about the coefficients of the polynomial velocity components (equation 7). Finally, the overall velocity profile is assumed to be a superposition of all the polynomial components of the voltage potentials (equation 8). Therefore, EVT provides the velocity distribution analytically for a continuous conductive phase in a circular pipe section, in either single phase or multiphase flow, essential to calculate the volumetric flowrate of the conducting phase.

III. Experimental Setup

A. Measurement Facility

The flow facility is a loop that allows a variety of fluids to be pumped through a 2m long vertical test section made of transparent perspex pipe with an ID of 80mm and OD of 90mm. This type of material is specifically chosen for the purpose of flow observations, and allows the MIT sensor to be clamped around the outside of the pipe non-intrusively. The mixture of fluids may contain water, oil or compressed gas. In this study, a type of non-hazardous silicone oil is used, which has a viscosity of 20Cst and a specific gravity of 0.95. The saline water has a conductivity of 35.0mS/cm. The MIT and EVT sensors are installed on a vertical section, with EVT sensor

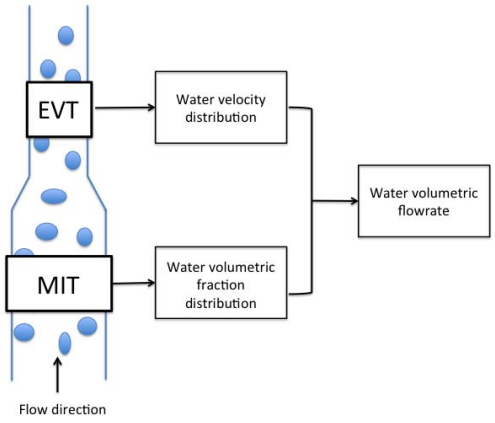

Fig. 1. Block diagram of instrumentation setup.

placed on top of the MIT sensor (Figure 1). The development length in the flow rig is 20 diameters at 80mm diameter, followed by a smooth conical contraction to 50mm diameter and a further 5 diameters of flow development before the EVT electrode ring. This arrangement is typical of oilfield-based venturi flowmeters where the average density is measured in the upstream portion of larger diameter. The water superficial velocity is $0.055m/s$ and the oil superficial velocity varies from $0.008m/s$ to $0.028m/s$ in the upstream 80mm pipe. Due to differences in pipe diameter, an assumption was made to calculate the equivalent local water velocity in the upstream 80mm section using the local water velocity in the 50mm section (equation 8). As both water and oil are incompressible and the temperature was kept constant, it was assumed that the variation of water density when moving downstream is negligible. Based on the flow continuity principles, the local water velocity in the upstream and downstream regions is proportional to the cross-sectional areas of both sections.

$$v_{w,upstream} = (\frac{r_{downstream}}{r_{upstream}})^2 v_{w,downstream} \tag{27}$$

As previously mentioned, both MIT and EVT are capable of real time flow imaging, i.e., continuous monitoring of the constituent properties of a multiphase flow (density, volumetric fraction and velocity). The aim of this paper is to measure the volumetric flowrate of the water phase, therefore the combination of MIT and EVT are used to measure the real time local water volumetric fraction and velocity distribution. Conventionally, for imaging based systems, the real time speed is usually defined by frames per second.

The MIT system utilises an array of 8 inductive coils to map the spatial distribution of the water phase in a multiphase flow. These coils are equally distributed on the periphery of the Perspex pipe. A signal generation unit passes an alternating current at 10MHz into one of the driving coils with the remaining coils acting as receivers to measure the induced voltages. This signal generation unit also has a data acquisition function, and interacts with a multiplexing control unit to switch coils sequentially. These measurements are then used for image reconstruction. This system is capable of real time imaging at 2 frames per second, where one frame involves the following, in order: coil excitation, measurement of voltage from receiving coils, data logging, data transfer to the host PC, image reconstruction and display. Although this rate is not yet sufficient for field applications, there is no theoretical objection to obtaining frame rates of several hundreds of frames per second in the future. The MIT sensors are packaged in a way to eliminate any external field perturbation, and to allow a direct clamp-on onto the flow loop. The same packaging is also used for electrical capacitance tomography sensors as reported elsewhere [37].

The EVT sensor is mounted on a vertical section of the flow loop with ID of 50mm. The front side of the 16 electrodes are exposed to the fluids via a "window", where all other sides are covered. This is not a completely contactless setup; nevertheless, the measuring operation remains non-intrusive, as the electrodes do not alter the constituencies within the fluids. Two Helmholtz coils are positioned to face each other directly. A power system is designed to supply and switch the voltages supplied to the coils at 2Hz, from a 48V DC power controlled solid-state relay network. As a consequence, a square wave magnetic field can be generated. 16 electrodes are equally spaced around the internal circumference of the pipe and measure the induced voltage potentials due to a conducting flow. Both the Helmholtz coil and the 16 electrodes are packaged in an aluminium case to allow a direct clamp-on onto the flow loop. The induced voltage potential measurements are passed into an electronics conditioning unit for noise filtration and signal amplification. The sensing package is connected to the electronics conditioning unit and eventually grounded to earth to prevent any cross-talk between the MIT sensor package. The filtered measurements are then used for reconstructing a velocity profile of the conducting phase. A system design can be found in [38], with a detailed diagram of the sensor design, circuits of the coil excitation and temperature compensation, as well as the circuit of the voltage measurement and control unit. This EVT system has a speed of 30 seconds per frame. Similarly, one frame involves the following, in order: driving both Helmholtz coils, measurement of the induced electric potential from all electrodes, data transfer to the host PC, reconstruction and display of the water velocity profile. This is a more severe restriction, and the present implementation is restricted to flows that are time-invariant.

As these two systems have different speeds, the measurements due to flow are recorded online so that the instantaneous water distribution and velocity can be displayed in real-time, although the integration of this information to obtain the water volumetric flowrate is calculated off-line. When conducting the experiments, one of the attempts to reduce the measurement error due to the time delay is to flow a certain mixture of water and oil at fixed rates for a long period of time to ensure a steady state of the flow was achieved, before altering the flow. After the steady flow condition is achieved, for each flow condition (Table II), the measurements are taken within 42s. In the integration (equation 26), for each frame of EVT water velocity distribution, the water volumetric fraction calculated from MIT is based on an average of 60 frames of data. Our in-house flow loop was also designed to facilitate

TABLE I
FLUID PROPERTIES

Fluid Properties	Silicone oil	Saline water
Density (kg/m^3)	970	1021
Dynamic Viscosity $(kg/m \cdot s)$	$1.94e^{-2}$	$1.00e^{-3}$
Conductivity (mS/cm)	0	35.0

TABLE II
MULTIPHASE FLOW CONDITIONS

Flow condition	$Q_{ref(w)}$ (m^3/s)	$Q_{ref(o)}$ (m^3/s)	water-in-liquid
(a)	$2.750e^{-4}$	$1.42e^{-4}$	65.80%
(b)	$2.750e^{-4}$	$0.92e^{-4}$	74.90%
(c)	$2.750e^{-4}$	$0.42e^{-4}$	86.78%
(d)	$2.750e^{-4}$	0	100%

this experimental process and ensure the flow status is well monitored and controlled by the reference flow meters.

B. Flow Conditions

The properties of the fluids used in this study are shown in Table I.

In this multiphase flow experiment, four flow conditions were tested, listed in Table II. The flowrate of the water and oil phase are measured directly before the mixing point, by a Key Instruments Flo-Rite FR2000 series clear acrylic reference flow meter for liquid, with a scale of 4-40 L/min (equivalent of $6.67e^{-5} - 6.67e^{-4} m^3/s$) and an accuracy of $\pm 5\%$ full scale. As water and oil have different density, both flowmeters have been calibrated on the flow rig for water and oil flow separately using a volumetric method, i.e., flowing a given fluid into a working section (with known pipe diameter), by measuring the flowing time (measured by a regular stopwatch) and the volume of the given fluid (the height of the standing column of fluid is recorded from a measuring tape), one can calculate the flowrate of the fluid. The ratio of the calculated flowrate to the indicated flowrate by the flowmeter is called the meter factor. This calibration practice is carried out 20 times prior to each multiphase flow experiment to track the meter factor and the final reference flowrate is obtained by multiplying the mean value of the meter factor with the indicated flowrate on a reference meter. The conductivity of the saline water is also measured before the mixing point, by a Hanna instruments HI-8733 portable multi-range conductivity meter. In this study the saline liquid has similar conductivity as that of produced water. As such, the measurement range of 0.0-199.9mS/cm is selected, with a resolution of $0.1 mS/cm$ and an accuracy of $\pm 1\%$ full scale.

IV. RESULTS

A. Visualisation of Multiphase Flows

The reconstructed water velocity distributions in Figure 2 a)-d) correspond to the flow conditions listed in Table II a)-d). The colour bar indicates the water velocity in metres per second, with blue showing low velocity and red showing high velocity. In the case of single phase flow, the flow pattern is axisymmetric (Figure 2 d), whereas the flow is no longer axisymmetric due to the presence of oil phase (Figure 2 a-c). One common feature in Figure 2 a)-c) is the existence of negative velocities. Negative continuous phase velocities are physically possible in two-phase flow, as the mixture density variations in the flow cross-section

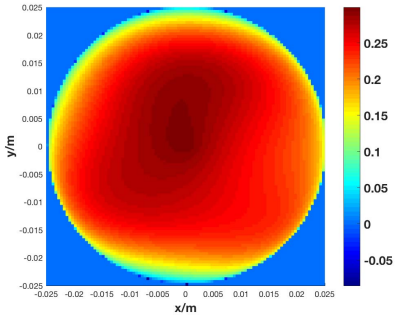

(a)

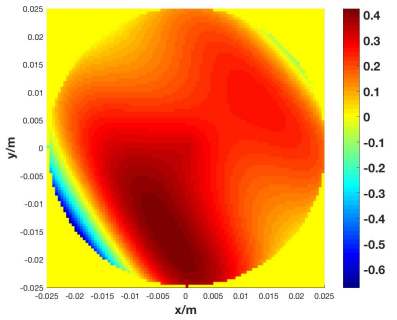

(b)

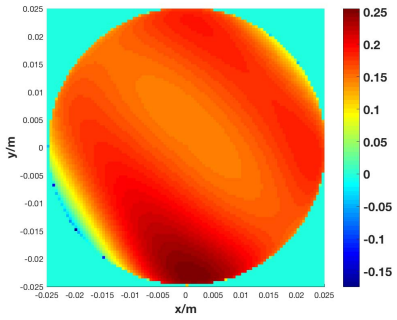

(c)

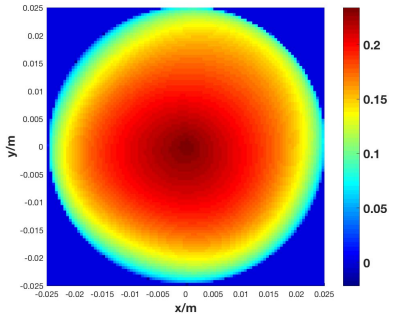

(d)

Fig. 2. Reconstructed water velocity distributions for flow conditions listed in Table II. The x- and y-axis show the pipe dimension in meter with the coordinates (x = 0, y = 0) being the center of the pipe, and the color bar in each figure shows the *in-situ* water velocity in m/s.

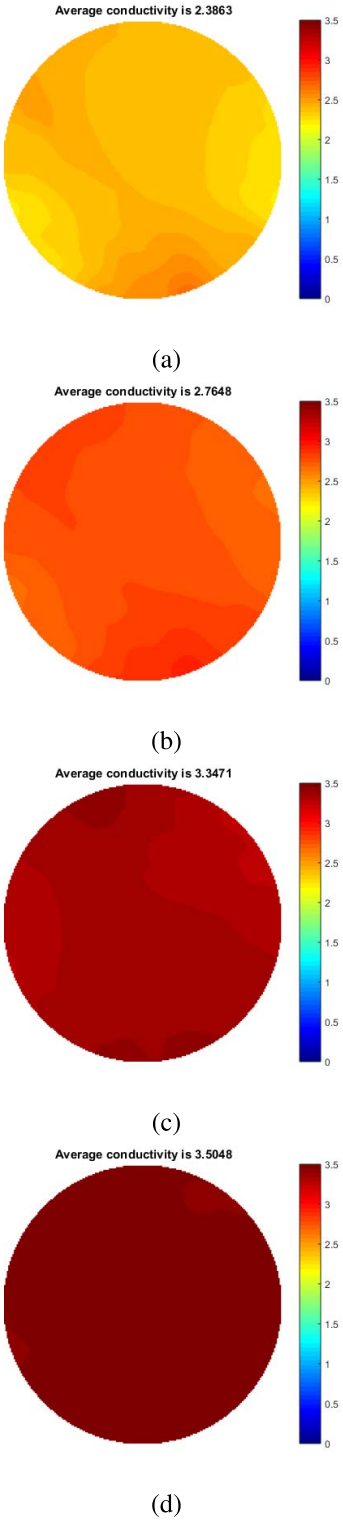

Fig. 3. Reconstructed conductivity images for flow conditions listed in Table II.

might result in the axial water velocity moving from positive (upward) values at the center of the pipe to negative (downward) values at the edges of the pipe. This flow behaviour has also been reported in [39]. The velocities shown here could suggest that the oil phase is more likely to be in the center of the pipe, whereas some water might be flowing towards the upstream $80mm$ section.

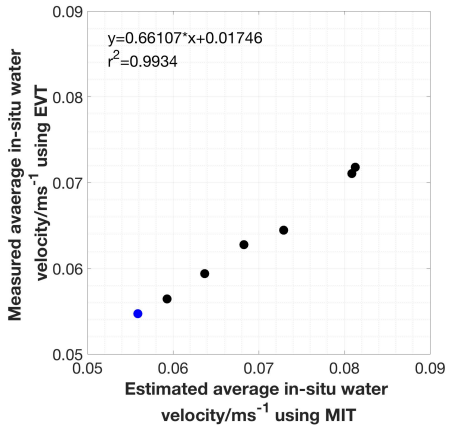

Fig. 4. Relationship of average in-situ water velocity obtained from MIT and EVT, where flow condition (d) - single phase water - is highlighted in blue.

The reconstructed images in Figure 3 reflect the reconstructed conductivity distribution for each of the flow conditions in Table II. The blue to red colour map is defined to show the conductivity distribution of the water phase, with blue showing zero conductivity and red showing the highest conductivity of $3.50S/m$. It is clear that as the water cut increases, the average conductivity increases, as it is also demonstrated in the change of the colour of these images.

B. Calculation of Water Volumetric Flowrate

For each of the multiphase flow condition listed in Table II, the experiments were conducted twice to evaluate the reproducibility. Figure 4 shows the relationship between the average in-situ water velocity directly measured by EVT using equation 8 and the average in-situ water velocity estimated using equation 18, in which the water volumetric fraction λ_w is obtained from MIT using equation 24 and 25. This means that the average water in-situ velocity can be obtained independently, as such the relationship between the velocities measured from EVT and MIT can be used as an indication of the overall system performance. Figure 4 shows these velocities are linear ($r^2 = 0.9934$).

Figure 5 shows percentage of water-in-liquid versus the calculated water volumetric fraction (from equation 25) and estimated slip velocity for various flow conditions. The slip velocity is calculated using equation 20, where the average oil in-situ velocity is calculated using equations 15, 19 and 24. As stated above, the water velocity can be obtained from both EVT and MIT independently, resulting in two sets of estimated slip velocity. It is clear that the calculated water volumetric fraction increases as the percentage of water-in-liquid increases, however the estimated slip velocity increases slightly first and then decreases. Overall the estimated slip velocities agree with each other. For relative higher water cut scenarios, the reproducibility of the data is relatively poorer in comparison with other flow conditions.

In here, we define the error as the difference between the calculated flowrate Q_w using equation 26 and the flowrate as determined by the reference flow meter Q_{ref}, i.e., water volumetric flowrate listed in Table II. Therefore relative error ζ

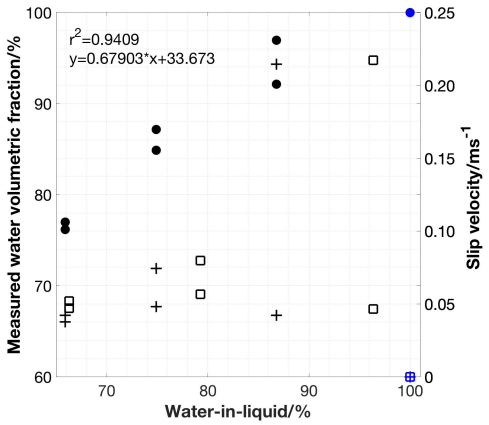

Fig. 5. Percentage of water-in-liquid versus calculated water volumetric fraction (shown in circles), and estimated slip velocities (with squares representing values calculated using MIT and crosses representing values calculated using EVT); where flow condition (d) - single phase water - is highlighted in blue.

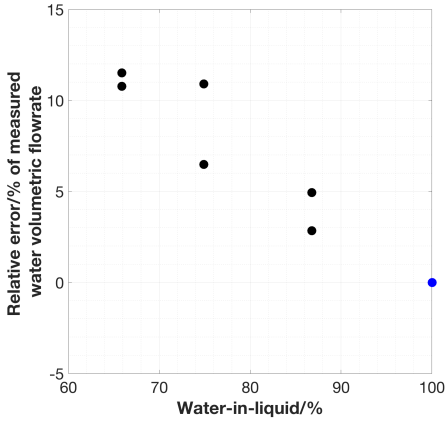

Fig. 6. Percentage of water-in-liquid versus relative error between calculated water flowrate and the reference water flowrate, where flow condition (d) - single phase water - is highlighted in blue.

is the error divided by the flowrate determined by the reference meter and is normally expressed as a percentage.

$$\zeta = \frac{Q_w - Q_{ref(w)}}{Q_{ref(w)}} \times 100\% \tag{28}$$

Figure 6 shows the percentage of water-in-liquid versus the relative error of calculated water volumetric flowrate. The relative error decreases as the water cut increases. The spread between two values for a given water-in-liquid percentage shows the reproducibility of the experiment for that particular flow condition, consistent with the spread observed in Figure 5.

C. Distribution of Water Volumetric Fraction and Velocity

To ensure the water volumetric fraction and velocity can be integrated properly, both the MIT and EVT sensing regions are divided by $p \times p$ number of pixels. The water distribution and velocity in each pixel can be calculated from equations 4 and 8. The normalised water volumetric fraction across the pipe can be obtained using $\sigma_{e,i_c,j=1:p}/max(\sigma_e)$. Similarly, the normalised water velocity can be written as $v_{w,i_c,j=1:p}/max(v_w)$. In both cases, index $i_{c,j=1:p}$ represents

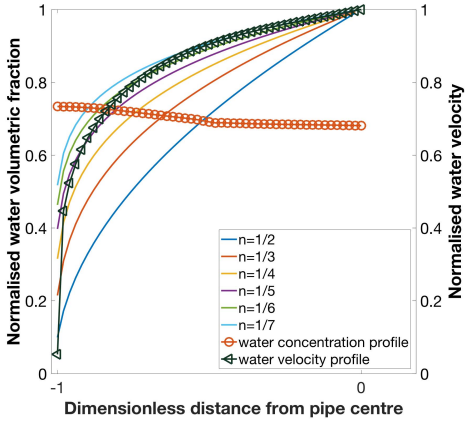

Fig. 7. Distribution of normalised water volumetric fraction and velocity profile from pipe periphery to pipe center for flow condition (a) in Table II.

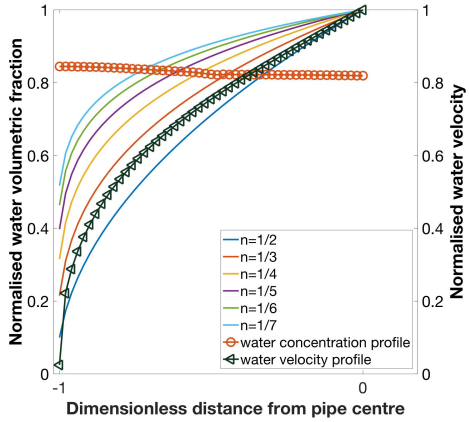

Fig. 8. Distribution of normalised water volumetric fraction and velocity profile from pipe periphery to pipe center for flow condition (b) in Table II.

the pixels that are located across the pipe. The purpose of this normalisation is to visualise both water volumetric fraction and velocity distribution in the same scale.

Figures 7 to 10 show the normalised water volumetric fraction and velocity distribution from the pipe periphery to the pipe center for flow conditions listed in Table II a)-d). A power law profile with exponent n can be used to characterise the shape of these velocity profiles, relatively low n values indicate a relatively flat profile whilst relatively higher values indicate a profile with a relatively pronounced peak at the pipe center [15]. The 2-D velocity profiles derived from the time-averaged velocity fields are shown in Figures 7 to 10. The flows here are two-phase with relatively short development lengths, but the range of power law exponents shown are consistent with a physically realistic range.

The water volumetric fraction profiles are fairly flat, with a tendency for there to be slightly more water towards the outside of the pipe, otherwise stated that the oil tends to flow in the center, consistent with Figure 2.

Figure 11 shows the percentage of water-in-liquid versus estimated flow distribution parameters. The flow distribution parameter is estimated using equation 21. Similarly, as there are two ways of obtaining the water in-situ velocity,

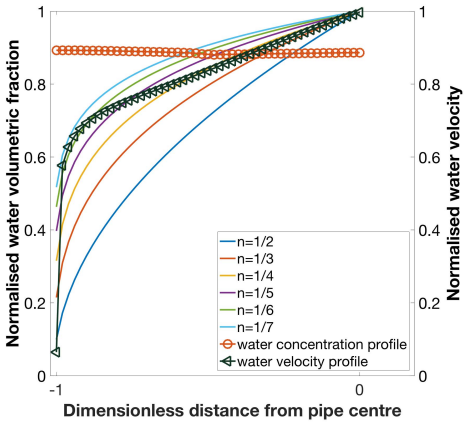

Fig. 9. Distribution of normalised water volumetric fraction and velocity profile from pipe periphery to pipe center for flow condition (c) in Table II.

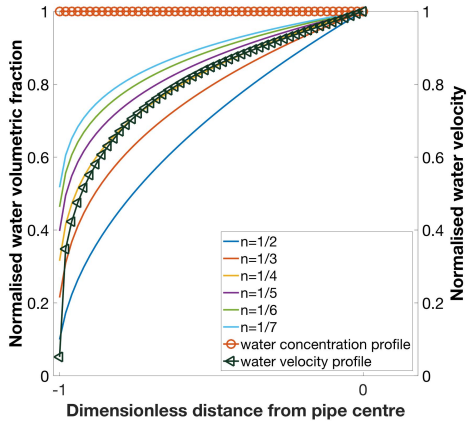

Fig. 10. Distribution of normalised water volumetric fraction and velocity profile from pipe periphery to pipe center for flow condition (d) in Table II.

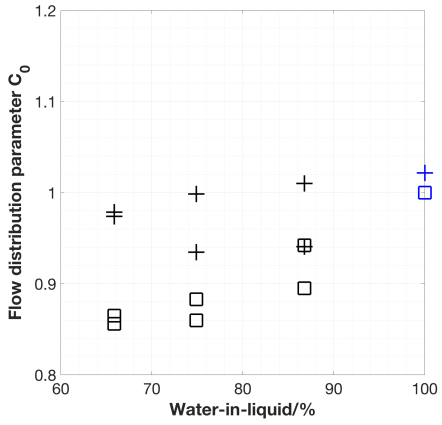

Fig. 11. Percentage of water-in-liquid versus estimated flow distribution parameters, (with squares representing values calculated using MIT and crosses representing values calculated using EVT); where flow condition (d) - single phase water - is highlighted in blue.

the estimated flow distribution for a given water-in-liquid percentage also has two sets of values. From the flowrate in Table II, the estimated flow distribution parameter C_0 can be close to 1 and even less than 1 [40], which are reflected in Figure 11.

V. Discussion

Considering first the velocity reconstructions from EVT, it can be seen that Figure 2 a)-c) show substantial non axisymmetric character, and substantially higher velocity compared to Figure 2 d) as the volumetric fraction of oil is decreased, thus decreasing the in-situ water velocity according to equations 18 and 25. It is also clear from Figure 2 d) that single-phase flow is essentially axisymmetric, with higher velocity distribution in the center and lower velocity distribution towards the pipe edge. In addition, one noticeable difference between the two-phase and single-phase cases is the presence of negative velocities in Figure 2 a)-c), suggesting that there is some recirculation as the oil phase slips faster locally through the water. The slip velocity is at its greatest at higher water-in-liquid ratios (Figure 5), presumably because the oil structure are less impeded in their motion by the constriction of other oil.

It should be noted that these contour plots are 'one-shot' single images. In a full implementation of an image-based flowmeter these individual profiles would be integrated with the water volumetric fraction profiles shown in Figure 3 at the same moment in time using equation 26, but in the experiments presented here the measurements are not co-located so that the integration has to be by time first, followed by later integration in space. Thus the experiments here can be used to characterise the likely character of typical current field systems, but there is an undefined uncertainty due to the integration process. Further work will place the image planes of velocity and volumetric fraction into close proximity where the integration can be more accurately performed.

The velocity profiles in Figure 7 to 10 show broad consistency with single-phase profiles, a turbulent $1/7$ power law profile at a Reynolds number of 4210 tending towards a center-peaked transitional flow at a Reynolds number of 2770 with power low exponent of $1/4$.

The in-situ water velocity as calculated by EVT is systematically lower than the equivalent velocity calculated from the reference flowmeter and the MIT estimate of water volumetric fraction (Figure 4). This means that the volumetric fraction of oil droplets decreases through the contraction and the slip velocity increases. The EVT data is after the contraction, and the resulting reduction in in-situ water velocity indicates an increase in water-in-liquid from 65.80% to 74.90%. This result is consistent with the model results presented in [41], where flow through a contraction is shown to increase the slip velocity between oil and water in a similar bubbly flow. Because both techniques used here give numerical information spatially across the cross-section of the flow, the calculation of drift-flux parameters is possible directly from the distributions. The physical test setup presented here is typical of a commercial venturi-based multiphase flowmeter, but not typical of published work on drift-flux correlations. However it can be said that the values calculated of distribution parameter and slip velocity are within the normal range of parameters expected.

Figures 7 to 10 show the normalised water volumetric faction across the pipe diameter as an example. In fact the

whole pipe areas are covered, i.e., one can obtain this information at any point in the pipe area. It is also feasible to measure the conductivity using either one or multiple pairs of contact or non-contact probe, and then derive the volumetric fraction directly, although these measurement techniques are not strictly tomographic (when compared to the summarised tomographic measurement processes in previous sections II-B, II-C and II-F). Within the MIT section, the flow distribution parameter is below 1, consistent with a distribution of water towards the outside of the pipe as shown in Figures 7 to 10, while the distribution parameter in the EVT section is close to 1. This indicates that the contraction, while tending to accelerate the lighter bubbly phase, also tends to lead to a more uniform distribution of that lighter bubbly phase across the flow.

For single-phase water flow, the direct water velocity measurements from the EVT system can be used to calculate the water volumetric flow rate. This flow rate is calibrated against the reference flow meter before each test to establish the meter factor. In this study, the relative error between the calculated and reference flow rate is 0.012% (Figure 6). This could be due to the velocity measurement error or could be within the reference flow meter accuracy. In this respect, in future studies, both the velocity and volumetric fraction will need to be validated against independent measurements. An uncertainty analysis for the complete system is also required to increase the measurement confidence level.

In addition, it is feasible to control the temperature in a laboratory condition, hence water density changes between the upstream and downstream region can be considered negligible. The local water velocity in the upstream can also be interpreted using the downstream velocity. This assumption arises from the rig setup, however there is no reason that both sections cannot be the same diameter. In future work, both sensors can be located more appropriately to improve measurement accuracy. Moreover, a temperature sensor could be beneficial for compensating the induced voltage changes if a more profound temperature change occurs along the vertical section.

Finally, the primary purpose of this work is to demonstrate the functional performance of the devices, and the test reference values are regarded as indicative only. It is not proposed that these results are calibrations - the conditions in the test section were complex developing multiphase flows where even the reference flowrates cannot completely define the flow: bubble size distribution, volume fraction, slip velocity and recirculation all being unknown and not amenable to other reference measurements. These parameters will vary considerably between calibration facilities and impact the accuracy and validity of calibrations undertaken. Future work will include traceable calibration of the test rig and devices under test. The contribution of this paper is to report developments that can help with quantitative assessment of the flow conditions used for calibration of conventional multiphase flow meters, and which offer a path to independent image-based flowmeters in the future.

VI. Conclusion

MIT and EVT can be used together in water continuous flows to measure the volumetric flowrate of the continuous water with a relative error between the calculated water flowrate and the reference water flowrate better than 1% for single-phase flow to 12% at 65.80% water-in-liquid multiphase flow. It is believed that the prime error is due to the fact that the measurements are not co-located so that the integration of flowrate is mathematically incorrect. However, this level of error is consistent with existing field-based multiphase flowmeters and with further work to co-locate the measurements, the error could be substantially reduced. The combination of EVT and MIT thus offers the opportunity of a robust, low-cost, non-radioactive alternative to current flowmeters at equivalent accuracy, while offering the potential for substantial improvement.

The instantaneous measurement of velocity profiles and volumetric fraction profiles offers the opportunity to further explore the fluid mechanics of complex flow systems, and to confirm the validity of computational models. The comparison with the drift-flux model presented here is a first example of this. The velocity profiles measured in the low-density contrast water-oil flows presented here, indicate similar trends to single-phase flows, though the flows cannot be considered to be homogenous as there is a significant slip velocity between the two phases.

The combination of techniques explored here considers the measurement of the continuous phase (water) in a two-phase flow (water-oil) where the material properties are known and invariant. Work is ongoing to add further measurement modalities which may enable full electromagnetic multiphase flow rate measurement for flows containing oil, gas and water. Comparisons will be made with other measurement techniques, with faster co-located measurements required for accurate real-time integration of flowrates.

Acknowledgment

The authors would like to thank the University of Huddersfield for providing the EVT system and software for this work.

References

[1] H. Jin, Y. Lian, S. Yang, G. He, and G. Guo, "The parameters measurement of air–water two phase flow using the electrical resistance tomography (ERT) technique in a bubble column," *Flow Meas. Instrum.*, vol. 31, pp. 55–60, Jun. 2013.

[2] J. G. Zhang and F. C. Ma, "Application of electrical resistance tomography to ice-water two-phase flow parameters measurement," *Key Eng. Mater.*, vols. 562–565, pp. 686–690, Jul. 2013.

[3] A. Hunt, J. Pendleton, and Y. Ladam, "Visualisation of two-phase gas-liquid pipe flows using electrical capacitance tomography," in *Proc. ASME 7th Biennial Conf. Eng. Syst. Design Anal.*, vol. 1, 2004, pp. 491–495.

[4] G. Costigan and P. B. Whalley, "Slug flow regime identification from dynamic void fraction measurements in vertical air-water flows," *Int. J. Multiphase Flow*, vol. 23, no. 2, pp. 263–282, 1997.

[5] J. G. Flores, X. T. Chen, C. Sarica, and J. P. Brill, "Characterization of oil-water flow patterns in vertical and deviated wells," *SPE Prod. Facilities*, vol. 14, no. 2, pp. 102–109, 1999.

[6] M. Fossa, "Design and performance of a conductance probe for measuring the liquid fraction in two-phase gas-liquid flows," *Flow Meas. Instrum.*, vol. 9, no. 2, pp. 103–109, 1998.

[7] R. A. Albrechtsen, Z. Z. Yu, and A. J. Peyton, "Preliminary experiments on the investigation of the inductive technique for measuring water content in multiphase flow," in *Proc. 4th Eur. Concerted Action Process Tomogr. Conf. (ECAPT)*, Bergen, Norway, Apr. 1995, pp. 205–213.

[8] Z. Liu, M. He, and H. Xiong, "Simulation study of the sensing field in electromagnetic tomography for two-phase flow measurement," *Flow Meas. Instrum.*, vol. 16, nos. 2–3, pp. 199–204, 2005.

[9] S. Watson, R. J. Williams, W. Gough, and H. Griffiths, "A magnetic induction tomography system for samples with conductivities below 10 S m^{-1}," *Meas. Sci. Technol.*, vol. 19, no. 4, p. 045501, 2008.

[10] L. Ma, A. Hunt, and M. Soleimani, "Experimental evaluation of conductive flow imaging using magnetic induction tomography," *Int. J. Multiphase Flow*, vol. 72, pp. 198–209, Jun. 2015.

[11] N. Terzija *et al.*, "Electromagnetic inspection of a two-phase flow of gainsn and argon," *Flow Meas. Instrum.*, vol. 22, no. 1, pp. 10–16, 2011.

[12] T. Wondrak *et al.*, "Combined electromagnetic tomography for determining two-phase flow characteristics in the submerged entry nozzle and in the mold of a continuous casting model," *Metall. Mater. Trans. B*, vol. 42, no. 6, pp. 1201–1210, 2011.

[13] H. Kanai, "The effects upon electromagnetic flowmeter sensitivity of non-uniform fields and velocity profiles," *Med. Biol. Eng.*, vol. 7, no. 7, pp. 661–676, 1969.

[14] B. Horner, F. Mesch, and A. Trächtler, "A multi-sensor induction flowmeter reducing errors due to non-axisymmetric flow profiles," *Meas. Sci. Technol.*, vol. 7, no. 3, pp. 354–360, 1996.

[15] G. P. Lucas, R. Mishra, and N. Panayotopoulos, "Power law approximations to gas volume fraction and velocity profiles in low void fraction vertical gas–liquid flows," *Flow Meas. Instrum.*, vol. 15, nos. 5–6, pp. 271–283, 2004.

[16] L. Xu, Y. Wang, and F. Dong, "On-line monitoring of nonaxisymmetric flow profile with a multielectrode inductance flowmeter," *IEEE Trans. Instrum. Meas.*, vol. 53, no. 4, pp. 1321–1326, Aug. 2004.

[17] O. Lehtikangas, K. Karhunen, and M. Vauhkonen, "Reconstruction of velocity fields in electromagnetic flow tomography," *Philos. Trans. Roy. Soc. A*, vol. 374, no. 2070, p. 20150334, 2016.

[18] L. E. Kollár, G. P. Lucas, and Z. Zhang, "Proposed method for reconstructing velocity profiles using a multi-electrode electromagnetic flow meter," *Meas. Sci. Technol.*, vol. 25, no. 7, p. 075301, 2014.

[19] Y. Muhamedsalih, G. P. Lucas, and Y. Q. Meng, "A two-phase flow meter for determining water and solids volumetric flow rates in stratified, inclined solids-in-water flows," *Flow Meas. Instrum.*, vol. 45, pp. 207–217, Oct. 2015.

[20] W. Yin and A. J. Peyton, "Sensitivity formulation including velocity effects for electromagnetic induction systems," *IEEE Trans. Magn.*, vol. 46, no. 5, pp. 1172–1176, May 2010.

[21] K. L. Ostrowski, S. P. Luke, and R. A. Williams, "Application of conjugate harmonics to electrical process tomography," *Meas. Sci. Technol.*, vol. 7, no. 3, pp. 316–324, 1996.

[22] J. A. Shercliff, *The Theory of Electromagnetic Flow-Measurement*. Cambridge, U.K.: Cambridge Univ. Press, 1987.

[23] R. S. MacTaggart, H. A. Nasr-El-Din, and J. H. Masliyah, "A conductivity probe for measuring local solids concentration in a slurry muxing tank," *Separat. Technol.*, vol. 3, no. 3, pp. 151–160, 1993.

[24] L. E. Kollär, G. P. Lucas, and Y. Meng, "Reconstruction of velocity profiles in axisymmetric and asymmetric flows using an electromagnetic flow meter," *Meas. Sci. Technol.*, vol. 26, no. 5, p. 055301, 2015.

[25] Y. Q. Meng and G. P. Lucas, "Imaging water velocity and volume fraction distributions in water continuous multiphase flows using inductive flow tomography and electrical resistance tomography," *Meas. Sci. Technol.*, vol. 28, no. 5, p. 055401, 2017.

[26] H. Li, M. Wang, Y.-X. Wu, and G. Lucas, "Volume flow rate measurement in vertical oil-in-water pipe flow using electrical impedance tomography and a local probe," in *Proc. 11th Int. Conf. Multiphase Flow Ind. Plants*, Palermo, Italy, 2008, pp. 293–302.

[27] R. W. Sillars, "The properties of a dielectric containing semiconducting particles of various shapes," *Inst. Elect. Eng.-Proc. Wireless Sec.*, vol. 12, no. 35, pp. 139–155, Jun. 1937.

[28] L. K. H. van Beek, "Dielectric behavior of heterogeneous systems," in *Progress in Dielectrics*, vol. 7, J. B. Birks, Ed. London, U.K.: Heywood, 1967, pp. 69–114.

[29] D. J. Jeffery, "Extension of the Maxwell-Wagner equation for conducting dielectrics," *J. Phys. D, Appl. Phys.*, vol. 9, no. 9, pp. L93–L95, 1976.

[30] A. Hunt, "Is electrical capacitance tomography ready for oilfield application?" in *Proc. SCADA*, Jun. 2012, pp. 13–14.

[31] H. Wu, C. Tan, X. Dong, and F. Dong, "Design of a conductance and capacitance combination sensor for water holdup measurement in oil–water two-phase flow," *Flow Meas. Instrum.*, vol. 46, pp. 218–229, Dec. 2015.

[32] J. E. Koskie, I. Mudawar, and W. G. Tiederman, "Parallel-wire probes for measurement of thick liquid films," *Int. J. Multiphase Flow*, vol. 15, no. 4, pp. 521–530, 1989.

[33] M. Wang *et al.*, "A new visualisation and measurement technology for water continuous multiphase flows," *Flow Meas. Instrum.*, vol. 46, pp. 204–212, Dec. 2015.

[34] M. Soleimani and W. R. B. Lionheart, "Absolute conductivity reconstruction in magnetic induction tomography using a nonlinear method," *IEEE Trans. Med. Imag.*, vol. 25, no. 12, pp. 1521–1530, Dec. 2006.

[35] H. Scharfetter, K. Hollaus, J. Rosell-Ferrer, and R. Merwa, "Single-step 3-D image reconstruction in magnetic induction tomography: Theoretical limits of spatial resolution and contrast to noise ratio," *Ann. Biomed. Eng.*, vol. 34, no. 11, pp. 1786–1798, 2006.

[36] M. Ziolkowski, S. Gratkowski, and R. Palka, "Solution of three dimensional inverse problem of magnetic induction tomography using Tikhonov regularization method," *Int. J. Appl. Electromagn. Mech.*, vol. 30, nos. 3–4, pp. 245–253, 2009.

[37] A. Hunt, "Weighing without touching: Applying electrical capacitance tomography to mass flowrate measurement in multiphase flows," *Meas. Control*, vol. 47, no. 1, pp. 19–25, 2014.

[38] Y. Zhao, G. P. Lucas, T. Leeungculsatien, and T. Zhang, "Measurement and control systems for an imaging electromagnetic flow meter," *ISA Trans.*, vol. 53, no. 2, pp. 423–432, 2014.

[39] T. Leeungculsatien and G. P. Lucas, "Measurement of velocity profiles in multiphase flow using a multi-electrode electromagnetic flow meter," *Flow Meas. Instrum.*, vol. 31, pp. 86–95, Jun. 2013.

[40] L. Haoues, A. Olekhnovitch, and A. Teyssedou, "Influence of the void fraction profile on the distribution parameter C_0 for a bubbly gas–liquid flow in a horizontal round pipe," *Nucl. Eng. Des.*, vol. 238, no. 4, pp. 1155–1158, 2008.

[41] B. Couët, P. Brown, and A. Hunt, "Two-phase bubbly-droplet flow through a contraction: Experiments and a unified model," *Int. J. Multiphase Flow*, vol. 17, no. 3, pp. 291–307, 1991.

Lu Ma received the B.Eng. and Ph.D. degrees in electronic and electrical engineering from the University of Bath, in 2011 and 2014, respectively. She subsequently joined iPhase Ltd., as the Principal Engineer, responsible for developing multiphase flow measurement techniques. She is currently a Post-Doctoral Researcher with the Engineering Tomography Laboratory, University of Bath. Her research interests include electrical imaging techniques, non-destructive evaluation, electromagnetics sensor and instrumentation, and multiphase flow measurement.

Dominic McCann received the B.Sc. (Hons.) degree in physics and computer science and the Ph.D. degree in physics from the University of Wales, Aberystwyth, in 1980 and 1983, respectively. He has more than 30 years' experience in technology development and commercialization in the oil and gas industry. He is currently the Managing Director of iPhase Ltd., which is developing the next-generation of multiphase flow meter (MPFM) that is based on electromagnetic imaging techniques. This instrument is the first MPFM that does not require a nuclear source or a Venturi. As a result, it will bring safety, operational performance, and cost benefits to the industry.

Andrew Hunt received the B.Sc. degree in engineering from Bristol University in 1978, and the Ph.D. degree from Cranfield University in 1982. He is currently a Professor of Oil and Gas Engineering with Coventry University, U.K. He is the Director and CTO of iPhase Ltd. and Atout Process Ltd. He has extensive research interests in flow measurement, process imaging, process nowcasting, and fluid mechanics.